

Bounds on the Fermion-Bulk Masses in Models with Universal Extra Dimensions

Gui-Yu Huang, Kyoungchul Kong

Department of Physics and Astronomy, University of Kansas, Lawrence, KS 66045 USA
E-mail: huang@ku.edu, kckong@ku.edu

Seong Chan Park

Department of Physics, Sungkyunkwan University, Suwon 440-746, Korea
E-mail: s.park@skku.edu

ABSTRACT: In models with extra dimensions, vectorlike Dirac masses for fermion fields are generically allowed. These masses are independent of electroweak symmetry breaking and do not contribute to the known masses for the quarks and leptons. They control the profile of the bulk wave functions, the mass spectra of Kaluza-Klein modes, and interactions that could be tested in experiments. In this article, we study the effects of bulk masses in electroweak precision measurements and in dark matter and collider searches, to set bounds on the bulk mass parameters in models with a flat universal extra dimension, namely, Split-UED. We find the current bound on the universal bulk-mass to be smaller than $(0.2-0.3)/R$, where R is the radius of the extra dimension. Similar but slightly relaxed bounds are obtained in the non-universal bulk mass case. The LHC is expected to play an important role in constraining the remaining parameter space.

KEYWORDS: Beyond Standard Model, Dark Matter, LHC, Extra Dimensions, Electroweak Precision Test, Bulk Mass, Split-UED.

Contents

1. Introduction	1
2. Universal Extra Dimensions with bulk fermion masses: split-UED	3
3. The Universal Case: $\mu_L = \mu_Q$	5
3.1 Oblique Corrections	5
3.2 Relic Abundance of KK Photon	8
3.3 Four Fermi Contact Interaction	10
3.4 Anomalous Muon Magnetic Moment	10
3.5 Collider Bounds	12
4. A Non-Universal Case: $\mu_L \neq \mu_Q$	14
4.1 Electroweak Precision Measurements: Oblique Corrections, Four Fermi Operators and Anomalous Magnetic Moment	15
4.2 Relic Abundance of KK Photon	16
4.3 Collider Bounds	17
5. Summary and Outlook	19

1. Introduction

As one of the most attractive extensions of the standard model (SM), extra dimensions have been extensively considered to address various problems in particle physics and cosmology. In particular, models with Universal Extra Dimensions (UED) [1] not only offer interesting dark matter phenomenology, but also predict signals that can be tested at colliders. Among many different scenarios, a 5-dimensional version, often referred to as Minimal Universal Extra Dimensions (MUED) [2,3], has been studied in detail (for reviews of the UED model and its phenomenology, see Ref. [4–6]). Recent studies on MUED suggest a lower bound of 700 GeV [7] on the KK mass scale $1/R$ (where R is the radius of the extra dimension) from the first year LHC data [8,9]. One also expects a relatively weak lower bound of $1/R \gtrsim 600$ GeV from flavor constraints [10], and $1/R \gtrsim 750$ (300) GeV for $m_h = 115$ (750) GeV [11–13] from electroweak (EW) precision measurements mainly due to the presence of (approximate) Kaluza-Klein (KK) number conservation and KK parity conservation. KK parity guarantees the stability of the lightest KK particle (LKP), thus providing a viable dark matter candidate [14,15]. In general, computation of relic abundance leads to an upper bound on the mass scale [14,16–20], resulting in a tension with electroweak constraints.

This tension may be relieved by considering effective coannihilation processes involving level-2 KK-leptons. A recent study [17] shows that the preferred dark matter scale in MUED could be increased to $1/R \simeq 1.4$ TeV, even though a high level of degeneracy, within a few percent, between the dark matter particle (level-1 KK state of $U(1)_Y$ gauge boson, B_1 or KK photon γ_1) and level-1 KK-leptons (ℓ_1) has to be realized. The high level degeneracy is a consequence of an assumption that brane localized operators at orbifold fixed points [21] as well as 5D fermion mass terms [22] are all vanishingly small, which leads us to another fine-tuning problem. Indeed, the dark matter and collider phenomenologies of UED models strongly depend on the detailed KK mass spectrum, which could be modified when either operators at the orbifold fixed points or 5D fermion mass terms are taken into account. In either case, not only the KK mass spectrum but also the KK particle couplings are significantly modified. In particular, the couplings of zero-mode fermions to even-numbered KK gauge bosons are generally non-zero, even at tree-level. Such couplings imply that higher KK modes can appear as resonances at the LHC [23–25].

Recently electroweak constraints on 5D fermion masses have been examined in Ref. [27] in a concrete context of Split Universal Extra Dimension (SUED) model [22]. For a large bulk mass ($\mu R \gtrsim 1$, where μ is the size of the bulk mass), the lower limit on the allowed KK mass scale, R^{-1} , is stronger than that in MUED, while close to the MUED limit ($\mu R \lesssim 1$), we notice that the corresponding lower bounds are relaxed allowing for lower KK mass scales. However it is important to compare with the preferred mass scale given by cosmological observations. A naive expectation is that once KK fermion masses become heavier than those in MUED, the annihilation cross sections of KK photon get suppressed by masses of the mediating KK fermions in the t - and u -channels, resulting in larger abundance hence lower KK scale. Therefore relic abundance requirement tends to lower the KK mass scale in the presence of fermion-bulk masses.

In this article, we consider constraints on fermion-bulk masses in SUED from various sources, such as relic abundance of dark matter, collider searches and electroweak precision measurements. We find that a tension between electroweak precision constraints and relic abundance still exists even in the presence of universal fermion-bulk mass. The tension may be weakened by introducing multiple fermion-bulk masses. It would be natural to have two different masses in hadronic and leptonic sectors, separately. Oblique corrections are mostly sensitive to KK tops due to a large Yukawa coupling, while the lepton sector may affect EW precision observables through the Fermi constant. Also the dominant contribution of relic abundance of KK photon dark matter comes from the lepton sector due to the nature of hypercharge interaction of the LKP. Finally, important collider limits in the presence of bulk masses arise differently from dijet and dilepton searches. For all these reasons, we consider a non-universal bulk mass case with two parameters. We consider a five dimensional version of SUED in this paper but expect that some of our results are still valid in different models with flat extra dimensions such as 6D UED, although additional constraints may arise.

We begin with a brief review on SUED in section 2, followed by discussions on various constraints for the universal case in section 3 and for the non-universal case in section 4. In each section we consider oblique corrections, relic abundance of KK photon, four Fermi

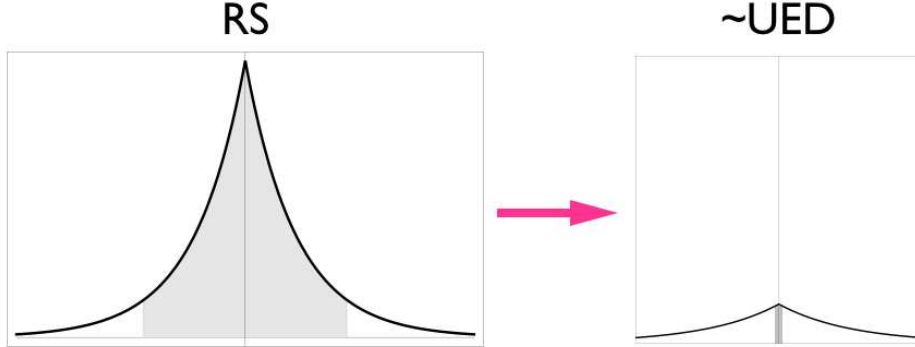


Figure 1: Schematic picture from Ref. [28] showing how integrating out parts of RS space yields an effective “UED” space.

interactions, anomalous muon magnetic moment and collider bounds. Section 5 is reserved for conclusions.

2. Universal Extra Dimensions with bulk fermion masses: split-UED

Here we provide a brief review on (Split) UED model with the exact KK-parity [22] following Ref. [28], where the model is understood as a low energy effective description of Randall-Sundrum (RS) model. The basic observation is that a \mathbb{Z}_2 symmetric space can be constructed by gluing two identical spaces together. The combined space is thus invariant under reflection about the midpoint. We can identify this \mathbb{Z}_2 reflection symmetry as the origin of KK parity. All SM particles are promoted to five dimensional fields propagating in this \mathbb{Z}_2 symmetric space.

As an explicit example, we glue two warped ‘throats’ together. After integrating out the middle portion corresponding to the highly warped UV-regime, as illustrated in Fig. 1, we obtain an effective geometry largely determined by the vicinity of the IR-boundaries, the near-flatness of which is desired for UED models. The integrating-out preserves the \mathbb{Z}_2 symmetry. Some phenomenological features of the two warped throat model were studied earlier in Refs. [29, 30].

In Split UED, Dirac masses for the fermions in the bulk are introduced for all fermions $\Psi = (Q, U, D, L, E)$

$$S_{\text{SUED}} \ni - \int d^4x \int_{-L}^L dy M_{\Psi}(y) \bar{\Psi} \Psi, \quad (2.1)$$

where the ‘size’ of the extra dimension is denoted by $L = \frac{\pi R}{2}$, and y is the coordinate of the extra dimension. With such a mass term, the fermion KK spectra can be significantly modified and *split* from those of the KK gauge bosons. To preserve KK parity, the y -dependent mass must be odd under reflection $M_{\Psi}(y) = -M_{\Psi}(-y)$ [22]. One notices that the mass term is compatible with *all* required symmetries of the model, namely, the 5D Lorentz symmetry, KK parity and also the gauge symmetries ($SU(3)_C \times SU(2)_W \times U(1)_Y$ in the minimal setup), so it is natural to be included. We choose the simplest kink-type mass, which may arise from

the minimum energy configuration with $w(y) \propto \tanh(my)$ in the large mass limit: $m \rightarrow \infty$, where $w(y)$ is the profile of the scalar field of mass m which is responsible for the fermion-bulk mass [31]

$$M_\Psi(y) = \mu_\Psi \tanh my \xrightarrow{m \rightarrow \infty} \mu_\Psi \theta(y) = \begin{cases} -\mu_\Psi & \text{if } y < 0 \\ +\mu_\Psi & \text{if } y > 0 \end{cases}. \quad (2.2)$$

In order to avoid the restrictive flavor bounds, we will assume one 5D mass for all quarks $-M_Q = M_U = M_D = \mu_Q \theta(y)$ and one for all leptons $-M_L = M_E = \mu_L \theta(y)$ following Refs. [22, 24], where in the universal bulk mass limit $\mu_L = \mu_Q \equiv \mu$.

Here we summarize some results from Refs. [22, 24], which are most relevant for our phenomenological study (for details, see the original references). The zero-mode fermions remain massless before electroweak symmetry breaking and obtain masses through Yukawa interactions. The mass of n -th KK level fermion follows from

$$m_{\Psi^{(n)}}^2 = \begin{cases} \lambda_\Psi^2 v^2 & \text{if } n = 0 \\ \mu^2 + k_n^2 + \lambda_\Psi^2 v^2 & \text{if } n \geq 1 \end{cases}, \quad (2.3)$$

where λ_Ψ is a Yukawa coupling and $v \approx 246$ GeV is the vacuum expectation value of the Higgs boson. The ‘momentum’ k_n is determined as

$$k_n = \begin{cases} \begin{cases} i\kappa_1 & : \kappa_1 = \kappa \in \{0 < \kappa \mid \mu = -\kappa \coth \kappa L, \mu L < -1\} \\ k_1 & : k_1 = k \in \{0 \leq k \leq \frac{\pi}{L} \mid \mu = -k \cot kL, \mu L \geq -1\} \end{cases} & \text{for } n = 1 \\ \frac{n}{R} = \frac{n\pi}{2L} & \text{for } n = 2, 4, 6, \dots \\ k_n = k \in \left\{ \frac{(n-2)\pi}{L} < k < \frac{(n-1)\pi}{L} \mid \mu = -k \cot kL \right\} & \text{for } n = 3, 5, 7, \dots \end{cases} \quad (2.4)$$

The coupling constants between the n^{th} KK gauge boson and m^{th} and ℓ^{th} KK fermions are determined by the overlap integral of the wave functions,

$$g_{m\ell n} = \frac{g_5}{\sqrt{2L}} \int_{-L}^L dy \psi_m(y) \psi_\ell^*(y) f_V^n(y) \quad (2.5)$$

$$\equiv g_{\text{SM}} \mathcal{F}_{m\ell}^n(\mu_\Psi L), \quad (2.6)$$

where $g_{\text{SM}} \equiv g_5/\sqrt{2L}$ is identified with the respective SM couplings and ψ_n (f_V^n) is the wave function of the n^{th} KK excitation of the fermion (vector boson). One immediately verifies that $\mathcal{F}_{00}^0 = 1$ irrespective of μ , as expected. We also emphasize that no KK number violating couplings exists between zero-mode gauge bosons and KK fermions (V_0 - f_n - f_ℓ) for $n \neq \ell$ as $\mathcal{F}_{n\ell}^0 = 0$. The zero-mode fermions do not couple to gauge bosons at odd KK levels, respecting KK parity. On the other hand, the coupling of the $(2n)^{\text{th}}$ gauge bosons to the SM fermion pair is allowed as [24]

$$g_{002n} = g_{\text{SM}} \mathcal{F}_{00}^{2n}(x_\Psi = \mu_\Psi L) \quad (2.7)$$

$$= g_{\text{SM}} \frac{x_\Psi^2 [1 - (-1)^n e^{2x_\Psi}] [1 - \coth(x_\Psi)]}{\sqrt{2(1 + \delta_{0n})} [x_\Psi^2 + n^2 \pi^2/4]}. \quad (2.8)$$

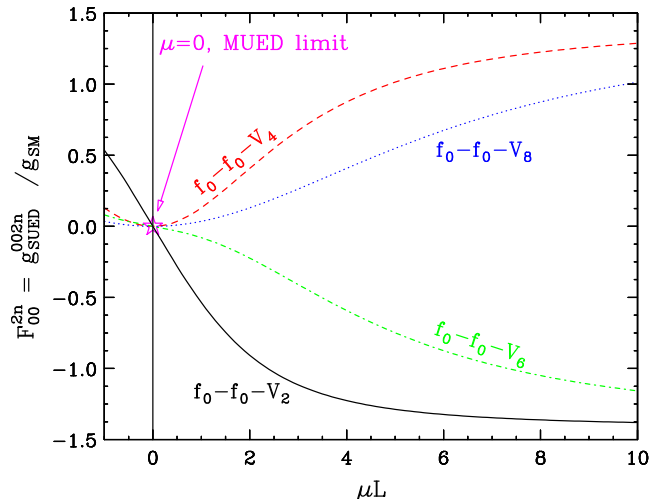


Figure 2: The ratio of tree-level couplings in SUED to the corresponding SM couplings.

A few examples of the $(2n, 0, 0)$ couplings are shown as functions of the bulk mass term in Fig. 2. The star (in magenta) represents the MUED limit ($\mu \rightarrow 0$) where those couplings vanish due to KK number conservation in MUED at tree level (later we mention loop-induced KK number violation). For $\mu \rightarrow \infty$, the zero mode fermions are well localized near the center ($y = 0$) so that their couplings to KK gauge bosons asymptotically approach the well known value $(-1)^n \sqrt{2}$ as one can see in Fig. 2. The alternating sign arises from the $2n$ -th KK gauge boson wave function which is proportional to $\cos n\pi = (-1)^n$ at $y = 0$ where the fermion wave function is mostly localized, while the $\sqrt{2}$ is from the zero mode normalization.

Many phenomenological aspects of SUED model have been explored, including dark matter [32], collider [24, 26, 32, 33], electroweak constraints [27] and flavor structure [28]. For studies on other varieties of UED models, see Refs. [34, 35].

In the following two sections we examine various constraints on the parameter space of Split UED. The two cases we study are one with a universal bulk mass, and the other with simplified non-universal bulk mass terms μ_Q and μ_L . We consider oblique corrections in terms of (S, T, U) parameters, the relic abundance of the KK dark matter, four Fermi contact interactions, anomalous magnetic moment of muon and also collider bound mainly from the recent LHC data.

3. The Universal Case: $\mu_L = \mu_Q$

3.1 Oblique Corrections

The constraints on the MUED model from electroweak precision tests have been studied in Refs. [11–13] by calculating the MUED contributions $(S, T, U)_{\text{UED}}$ to the oblique parameters

[36] at one loop-level. The leading contributions are found in Refs. [11–13]:

$$S_{UED} = \frac{4 \sin^2 \theta_W}{\alpha} \left[\frac{3g^2}{4(4\pi)^2} \left(\frac{2}{9} \sum_n \frac{m_t^2}{(n/R)^2} \right) + \frac{g^2}{4(4\pi)^2} \left(\frac{1}{6} \frac{m_h^2}{1/R} \right) \zeta(2) \right], \quad (3.1)$$

$$T_{UED} = \frac{1}{\alpha} \left[\frac{3g^2}{2(4\pi)^2} \frac{m_t^2}{m_W^2} \left(\frac{2}{3} \sum_n \frac{m_t^2}{(n/R)^2} \right) + \frac{g^2 \sin^2 \theta_W}{(4\pi)^2 \cos^2 \theta_W} \left(-\frac{5}{12} \frac{m_h^2}{1/R} \right) \zeta(2) \right], \quad (3.2)$$

$$U_{UED} = -\frac{4 \sin^2 \theta_W}{\alpha} \left[\frac{g^2 \sin^2 \theta_W}{(4\pi)^2} \frac{m_W^2}{(1/R)^2} \left(\frac{1}{6} \zeta(2) - \frac{1}{15} \frac{m_h^2}{(1/R)^2} \zeta(4) \right) \right], \quad (3.3)$$

where θ_W is the Weinberg angle, g is the coupling strength of $SU(2)_W$ interaction, and $\alpha = e^2/4\pi$ is the fine structure constant, and m_t , m_W and m_h are masses of the top, W and Higgs in the SM, respectively. $\zeta(n)$ is the Riemann zeta function. We neglect the small radiative corrections to KK masses. The terms proportional to the Riemann zeta functions arise from summations over all KK Higgs and KK gauge boson loops. Summation over KK tops is shown explicitly above for further discussion. All other KK fermion loops are neglected due to fermion mass suppression. For $m_h = 120$ GeV, oblique corrections in MUED lead to $R^{-1} \gtrsim 700$ GeV at 95% Confidence Level (C.L.).

In Split UED, there appear additional corrections to the parameters via KK W contributions to the Fermi constant [27],

$$G_F = G_F^0 + \delta G_F, \quad (3.4)$$

$$G_F^0 = \frac{g^2}{\sqrt{32} m_W^2}, \quad (3.5)$$

$$\delta G_F = \frac{1}{\sqrt{32}} \sum_n \frac{g_{002n}^2}{m_W^2 + \left(\frac{2n}{R}\right)^2}, \quad (3.6)$$

where g_{002n} is defined earlier in Eq. (2.8). Treating the leptonic and hadronic sectors universally, $\mu = \mu_L = \mu_Q$ as in Ref. [27], one can express the oblique parameters as follows [37]:

$$\begin{aligned} S_{SUED} &= S_{UED}, \\ T_{SUED} &= T_{UED} - \frac{1}{\alpha} \frac{\delta G_F}{G_F}, \\ U_{SUED} &= U_{UED} + \frac{4 \sin^2 \theta_W}{\alpha} \frac{\delta G_F}{G_F}. \end{aligned} \quad (3.7)$$

Here the following substitution of the fermion KK tower summations in the $(S, T, U)_{UED}$ is understood:

$$\sum_n \frac{m_f^2}{(n/R)^2} \rightarrow \sum_n \frac{m_f^2}{\mu^2 + k_n^2 + m_f^2}, \quad (3.8)$$

where k_n is defined in Eq. (2.4).

In Fig. 3, we show the electroweak constraints in Split UED for a universal bulk mass by tracing the 65% (dotted), 95% (dashed) and 99% (solid) C.L. fit contours (in blue) in

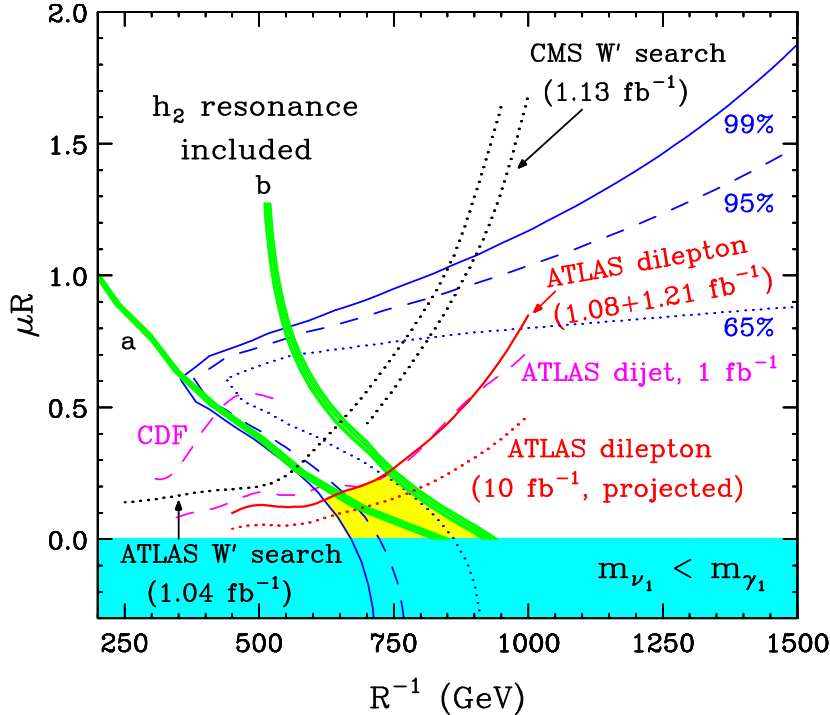


Figure 3: Constraints from relic abundance (in green, $\Omega h^2 = 0.1123 \pm 0.0035$), electroweak precision measurements (in blue) and collider search (in black, red, and magenta) in the Split UED parameter space for the universal bulk mass. Contours of EW constraints correspond to the 65% (dotted), 95% (dashed) and 99% (solid) C.L. fits for the oblique parameters. $\mu < 0$ leads to KK-neutrino DM, which is unviable as a dark matter candidate. The h_2 resonance is included in ‘b’, while only self-annihilation of KK photon contributes in ‘a’. Collider constraints shown are the current limits from ATLAS and CMS W' (dotted black), ATLAS dilepton (solid red), as well as the projected 10 fb^{-1} reach (dotted red) of the ATLAS dilepton search. Current CDF and ATLAS limit from dijet search are shown in dashed-magenta curves.

the (μ, R^{-1}) space, which is consistent with results in Ref. [27]¹. We used the following experimental bounds on new physics contributions to the oblique parameters: $S_{NP} = 0.04 \pm 0.10$, $T_{NP} = 0.05 \pm 0.11$, $U_{NP} = 0.08 \pm 0.11$, for a reference point $m_h = 120 \text{ GeV}$ and $m_t = 173 \text{ GeV}$ with correlation coefficients of $+0.89$ (-0.45 , -0.69) between S_{NP} and T_{NP} (S_{NP} and U_{NP} , T_{NP} and U_{NP}), which have recently been updated by the *Gfitter* collaboration [13].

Constraints on R^{-1} become stronger than in MUED for a large value of μ ($\mu R \gtrsim 1$) due to enhancement in couplings of level- $2n$ gauge mode to SM fermion pair (see Eqs. (2.7)-(2.8)). It is interesting to notice that the lower bound on KK mass scale in MUED, $R^{-1} \gtrsim 700 \text{ GeV}$, is reduced for $\mu R < 1$. At $\mu R \sim 0.6$, the EW constraints lead to the minimum allowed value of $R^{-1} \gtrsim 400 \text{ GeV}$.

¹We represent our results in the $(\mu R, R^{-1})$ space for easy comparison with results in Ref. [27]. However we find it more convenient to use $\mu L = \mu R \frac{\pi}{2}$ instead of μR . Therefore we use μL in all figures except Fig. 3.

3.2 Relic Abundance of KK Photon

As discussed in the introduction, annihilation cross sections are reduced due to the heaviness of KK fermions in the t - and u -channels, leading to larger relic density thus lower LKP mass, to keep consistency with cosmological observations. Hence it is important in SUED to take into account different KK fermion masses, when computing relic abundance. The masses of level-1 KK fermions are given by $m_1 = \sqrt{k_1^2 + \mu^2}$ in the absence of loop corrections ignoring EW symmetry breaking effect (see Eq. (2.3)). For $\mu \neq 0$, KK fermions are heavier than KK photon, $m_{f_1} > m_{\gamma_1} \approx R^{-1}$. Without an s -channel resonance, non-relativistic velocity expansion

$$\sigma_{tree} v = a + b v^2 + \mathcal{O}(v^4), \quad (3.9)$$

is a good approximation to obtain relic density [14] and we take two leading terms in the annihilation cross sections from Ref. [16]. For tree-level annihilation cross section via KK fermion exchange, they are

$$a = \sum_f \frac{32\pi\alpha_Y^2 N_c m_{\gamma_1}^2}{9} \left(\frac{Y_{fL}^4}{(m_{\gamma_1}^2 + m_{f_{L1}}^2)^2} + \frac{Y_{fR}^4}{(m_{\gamma_1}^2 + m_{f_{R1}}^2)^2} \right), \quad (3.10)$$

$$b = - \sum_f \frac{4\pi\alpha_Y^2 N_c m_{\gamma_1}^2}{27} \left(Y_{fL}^4 \frac{11m_{\gamma_1}^4 + 14m^2 m_{f_{L1}}^2 - 13m_{f_{L1}}^4}{(m_{\gamma_1}^2 + m_{f_{R1}}^2)^4} + Y_{fR}^4 \frac{11m_{\gamma_1}^4 + 14m_{\gamma_1}^2 m_{f_{L1}}^2 - 13m_{f_{L1}}^4}{(m_{\gamma_1}^2 + m_{f_{R1}}^2)^4} \right), \quad (3.11)$$

where $\alpha_Y = g'^2/4\pi$ with g' being the $U(1)_Y$ hypercharge gauge coupling, and $N_c = 3(1)$ for f being quark (lepton). Y_f is the hypercharge of the fermion f . f_{L1} (f_{R1}) represents $SU(2)_W$ -doublet (singlet) KK fermion at level-1. The contribution from the Higgs final states remains the same as in MUED.

Results from the relic abundance constraint ($\Omega h^2 = 0.1123 \pm 0.0035$) are shown in Fig. 3 in the SUED parameter space with a universal bulk mass, represented as the green band ‘a’ (‘b’) without (with) resonance annihilation of KK photons through h_2 [20]. The thickness in the green bands corresponds to uncertainty in Ωh^2 . In principle, R^{-1} lower than the bands is still allowed for $\Omega h^2 < 0.1123$ but other source of DM abundance is needed to account for the deficit. A 5D fermion mass parameter $\mu < 0$ leads to a LKP which is the KK partner of a SM neutrino and does not provide a viable dark matter candidate [24, 38]. Unlike the non-trivial behavior in oblique corrections, the lower bound on the preferred range of R^{-1} from relic abundance decreases monotonically when μ increases.

There are two important corrections to the relic abundance of KK photon. First, coannihilation processes are important in MUED [14, 16] due to the mass degeneracy. Specifically, coannihilations with $SU_W(2)$ -singlet leptons reduce the LKP mass, while coannihilation processes with other KK particles tend to increase it. Second, KK resonance at level-2 play an important role and increase the KK mass scale significantly [20]. In MUED, the mass splitting between level-2 KK Higgs and KK photon is about 1-2% for most of the allowed

parameter space and the corresponding enhancement in the relic abundance is $\sim 30\%$. The improved analysis including coannihilation processes can be found in Ref. [19]. Resonance effects of other level-2 KK particles are studied in Ref. [18]. It is also noticed in Ref. [17] that when allowing level-2 particles in the final state, mainly γ_2 and h_2 , the relic abundance decreases sharply, shifting the preferred value of the dark matter mass above the TeV scale. This is due to the important contribution of the coannihilation channels ($\ell_1\gamma_1 \rightarrow \ell\gamma_2$) that are enhanced by the exchange near resonance of the level-2 KK singlet lepton. All these resonance effects tend to increase the mass scale of KK photon, while coannihilations with $SU(2)_W$ -singlet leptons tend to move in the opposite way. Results in MUED from Ref. [17], for $m_h = 120$ GeV, $\Lambda R = 20$ and $R^{-1} = 1$ TeV, show that the relative contributions to Ωh^2 are $\gamma_1\ell_1 \sim 0.6$, $\ell_1\ell_1 \sim 0.13$, $\gamma_1 h_1 \sim 0.09$, $\gamma_1\gamma_1 \sim 0.06$, $\ell_1 h_1 \sim 0.05$, $V_1 h_1 \sim 0.02$, $h_1 h_1 \sim 0.02$, $\gamma_1\ell_1 \sim 0.017$, and $V_1\ell_1 \sim 0.01$, among which all fermion initial states are negligible for a sizable bulk mass in SUED. The remaining important processes are then $\gamma_1 h_1$, $\gamma_1\gamma_1$, $V_1 h_1$ and $h_1 h_1$. Among them, $\gamma_1 h_1$ and $\gamma_1\gamma_1$ are the dominant processes to determine the relic abundance.

In our study, we do not include coannihilation processes among KK fermions and KK photon since there can be a relatively large mass gap in the presence of a bulk mass. They become important only when $\mu R \lesssim 0.01$, i.e., near the MUED limit. It is essentially the size of 1-loop radiative corrections in MUED, where the correction to masses of $SU(2)_W$ -singlet KK leptons is $\sim 1\%$. For the same reason, we do not include processes such as $\ell_1\ell_1 \rightarrow Z_2(\gamma_2)$, $\nu_1\ell_1 \rightarrow W_2$, $\ell_1\gamma_1 \rightarrow \ell_2\ell_0$ etc. However, we attempt to include some effects of h_2 resonance in $\gamma_1\gamma_1 \rightarrow h_2$, although the bosonic sector may or may not stay the same as in MUED. Following the procedure described in Ref. [20], we have numerically integrated the thermally averaged cross section including the Higgs resonance (σ_{res})². The improved relic abundance including h_2 resonance is labeled as ‘b’ in Fig. 3. Other coannihilation processes with KK bosons such as $\gamma_1 h_1^\pm \rightarrow (W_2^\pm, h_2^\pm)$, $\gamma_1 h_1 \rightarrow (A_2, \gamma_2, Z_2)$, $A_1 A_1 \rightarrow h_2$, $h_1^+ h_1^- \rightarrow (h_2, Z_2, \gamma_2)$ etc may still contribute to the final relic abundance in principle [18]. In the absence of a complete knowledge of the mass spectrum, our results are valid in the limit where all KK bosons other than the KK photon are heavy and decoupled from the relic abundance calculation. These estimates should provide a ballpark range, since resonance effects in the coannihilations are known to be less than about 30% in MUED [18]. One should revisit more systematically with radiatively corrected KK masses, which is not known currently.

The bulk mass parameter μ can also be constrained from below by dark matter direct detection experiments. The main process involves the s - and t -channel exchange of KK quarks at level-1 (q_1) between KK photon γ_1 and the nucleus. Current limit from XENON100 [39] data implies a lower limit of $\mu R \gtrsim 0.01$, which is not shown in our plot. At small μQ , q_1 and γ_1 are nearly degenerate, and the direct detection cross section is enhanced resonantly. Our calculation does not include a full treatment of radiative corrections to the mass spectrum nor the finite width effect.

²We have used the decay width of the h_2 in MUED, which should be a good approximation for $\mu R < 1$. For the purpose of setting bounds on μ , this is acceptable since LHC already constrain $\mu R < 0.2 \sim 0.3$, as we will see later.

In summary, coannihilation effect with KK leptons are negligible for a large bulk mass and the effect with level-2 final states are expected to be small. We considered the Higgs resonance effect as shown in Fig. 3. This constraint on the dark matter abundance sets an upper limit on R^{-1} .

3.3 Four Fermi Contact Interaction

In UED models, the Kaluza-Klein weak gauge bosons can contribute to the four Fermi contact operators, which can be constrained by the experiments. We consider lepton-lepton, lepton-quark and quark-quark contact interactions which are described by the effective operators of the form of $\ell\bar{\ell}\ell\bar{\ell}$, $e\bar{e}q\bar{q}$ and $q\bar{q}q\bar{q}$, respectively, with $\ell = e, \mu, \tau$ [40]. It turns out the most stringent bound arises from the electron-quark contact interactions of the form of $e\bar{e}u\bar{u}$ and $e\bar{e}d\bar{d}$ (see Table 1) for $\mu_L = \mu_Q = \mu$ with $\eta_{AB}^q = \pm 1$:

$$\mathcal{L}_{\text{eff}}^{eq} \ni \sum_{q=u,d} \sum_{\{A,B\}=\{L,R\}} \frac{4\pi}{\Lambda_{q,AB}^2} \eta_{AB}^q \bar{e}_A \gamma^\mu e_A \bar{q}_B \gamma_\mu q_B, \quad (3.12)$$

where

$$\frac{4\pi}{\Lambda_{q,AB}^2} \eta_{AB}^q = 4\pi N_c \sum_{n=1}^{\infty} (\mathcal{F}_{00}^{2n}(\mu R))^2 \times \left[\frac{3}{5} \frac{\alpha_1 Y_{e_A} Y_{q_B}}{Q^2 - M_{B_{2n}}^2} + \frac{\alpha_2 T_{e_A}^3 T_{q_B}^3}{Q^2 - M_{W_{2n}^3}^2} \right] \quad (3.13)$$

$$\approx -\pi N_c R^2 \left(\frac{3}{5} \alpha_1 Y_{e_A} Y_{q_B} + \alpha_2 T_{e_A}^3 T_{q_B}^3 \right) \times \sum_{n=1}^{\infty} \frac{(\mathcal{F}_{00}^{2n}(\mu R))^2}{n^2}, \quad (3.14)$$

for a KK scale which is larger than the momentum transfer, $1/R \gg Q^2$. Here $N_c = 3$ is the color factor ($N_c = 1$ for $\ell\bar{\ell}\ell\bar{\ell}$ type contact interactions), and Y 's and T 's are the hypercharges and isospins of the corresponding fermions. We take $m_{B_{2n}}^2 \approx m_{W_{2n}^3}^2 \approx (2n/R)^2$, considering $(m_W R)^2 \ll 1$. The RG running effect of gauge couplings is included as well:

$$\alpha_1(\mu) = \frac{5}{3} \frac{g'^2(\mu)}{4\pi} = \frac{\alpha_1(m_Z)}{1 - \frac{b_1}{4\pi} \alpha_1(m_Z) \log \frac{\mu^2}{m_Z^2}}, \quad (3.15)$$

$$\alpha_2(\mu) = \frac{g^2(\mu)}{4\pi} = \frac{\alpha_2(m_Z)}{1 - \frac{b_2}{4\pi} \alpha_2(m_Z) \log \frac{\mu^2}{m_Z^2}}, \quad (3.16)$$

with $\alpha_1(m_Z) \approx 0.017$, $\alpha_2(m_Z) \approx 0.034$, and $(b_1, b_2) = (41/10, -19/6)$. We find that the contact interaction yields quite strong constraints for $1/R$ as shown in Fig. 4, and is comparable (slightly better large R^{-1}) to limits in the W' searches at the LHC. However we do not show this limit in Fig. 3, as the LHC limit is stronger. Note that $\mu L = \mu R \frac{\pi}{2}$.

3.4 Anomalous Muon Magnetic Moment

In a previous study of MUED, the leading order correction to the anomalous magnetic moment of muon at 1-loop level is obtained [42]:

$$\Delta a_\mu^{\text{MUED}} \simeq \frac{\alpha}{8\pi} \sum_n \frac{(m_\mu R)^2}{n^2} \{C_V + C_5\}, \quad (3.17)$$

Table 1: Four Fermi contact interaction bounds in PDG(2010) [41].

TeV	$eeee$	$ee\mu\mu$	$ee\tau\tau$	$llll$	$qqqq$	$eeuu$	$eedd$
Λ_{LL}^+	> 8.3	> 8.5	> 7.9	> 9.1	> 2.7	> 23.3	> 11.1
Λ_{LL}^-	> 10.3	> 9.5	> 7.2	> 10.3	2.4	> 12.5	> 26.4

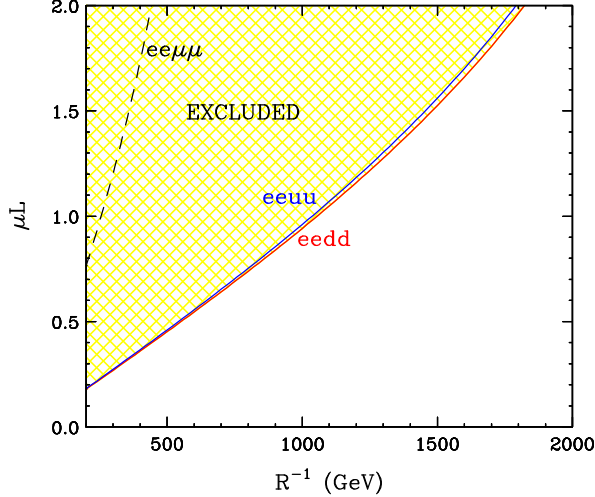


Figure 4: The four Fermi interaction excludes the upper-left corner of the μ_L - R^{-1} plane.

where m_μ is the mass of muon and $C_\mu(C_5)$ stands for the effective coupling of the vector (the fifth) components of the KK gauge bosons and Goldstone modes with the zero mode muon, which can be conveniently written separately:

$$C_{V^{(5)}} = (C_{A^{\mu(5)}} + C_{Z^{\mu(5)}} + C_{W^{\mu(5)}}), \quad (3.18)$$

$$C_{A^\mu} = \frac{2}{3} = -\frac{2}{3}C_{A_5}, \quad (3.19)$$

$$C_{Z^\mu} = -\frac{3 + 4\sin^2\theta_W \cos 2\theta_W}{3\sin^2 2\theta_W}, \quad (3.20)$$

$$C_{Z^5} = \frac{1 + 12\sin^2\theta_W \cos 2\theta_W}{6\sin^2 2\theta_W}, \quad (3.21)$$

$$C_{W^\mu} = 2C_{W^5} = -C_{G^\pm} = -\frac{1}{3\sin^2\theta_W}. \quad (3.22)$$

We also include the Goldstone contribution (C_{G^\pm}). Taking $\alpha(m_Z) = 1/127$ and $\sin^2\theta_W = 0.2316$, we get $\Delta a_\mu^{\text{MUED}} \approx -1.2 \times 10^{-11}$ for $R^{-1} = 1$ TeV, which is far below the detectable range. Given that KK fermions are heavier in SUED, the contributions are doubly suppressed by the fermion masses and by the coupling constants ($\sim g_{\text{SM}}\mathcal{F}_{n0}^n$). We found that the contribution from the KK number conserving interactions in SUED could be reduced down to 61% (17%) of the value in MUED when $\mu_L L = 1.0$ (3.0).

However, in SUED there are potentially more important KK number violating contributions from loops containing the $(2n)^{\text{th}}$ neutral KK gauge bosons, i.e., B_{2n} and W_{2n}^3 , as the zero mode muon has sizable couplings to them ($\sim g_{\text{SM}} \mathcal{F}_{00}^{2n}$):

$$\Delta a_{\mu}^{B_{KK}} \simeq -\frac{3\alpha_1}{16\pi} \cdot (m_{\mu}R)^2 \sum_n \left(\frac{\mathcal{F}_{00}^{2n}}{n} \right)^2 \times L_1, \quad (3.23)$$

$$\Delta a_{\mu}^{W_{KK}^3} \simeq -\frac{\alpha_2}{16\pi} \cdot (m_{\mu}R)^2 \sum_n \left(\frac{\mathcal{F}_{00}^{2n}}{n} \right)^2 \times L_2. \quad (3.24)$$

Here $L_i = \frac{1}{2} \int_0^1 dx \frac{Q_i(x)}{1-x+\lambda_n^2 x^2}$ is the loop functions with $\lambda_n = \frac{m_{\mu}}{m_{2n}} \approx \frac{m_{\mu}R}{2n}$, $Q_{B_{2n}}(x) = Q_V(x)$ and $Q_{W_{2n}^3}(x) = Q_V(x) - Q_A(x)$. The vector and axial vector coupling functions are $Q_V(x) = 2x^2(1-x)$ and $Q_A(x) = 2x(1-x)(x-4) - 4\lambda_n^2 x^3$, respectively. Explicitly, $L_1 = 1/3$ and $L_2 = 2$ when we take $\lambda_n = 0$ for the integration [43]. Finally, the leading contribution³ from the neutral KK bosons is estimated as

$$\Delta a_{\mu}^{\text{SUED}} \approx -1.8 \times 10^{-11} \left(\frac{1 \text{ TeV}}{R^{-1}} \right)^2 \sum_n \left(\frac{\mathcal{F}_{00}^{2n}}{n} \right)^2, \quad (3.25)$$

where $\sum_n \left(\frac{\mathcal{F}_{00}^{2n}}{n} \right)^2 < 2$ for $\mu_L L < 5$, which is still too small to be detected. This new contribution vanishes in the MUED limit where $\mathcal{F}_{00}^{2n} \rightarrow 0$.

3.5 Collider Bounds

In MUED, the first level of KK excitations can be produced in pairs at colliders, with the typical missing energy signature due to conservation of KK parity. Recent studies indicate a bound of $1/R \gtrsim 700 \text{ GeV}$ [7] for MUED from the first year LHC data. While KK parity in UED is conserved, KK number is broken through loop-generated couplings between level-2 KK bosons and SM fermion pairs. These KK bosons can appear as resonances in the dilepton or dijet final states, but their productions are heavily suppressed by loop factors.

In SUED, however, these couplings exist at tree-level in the presence of μ . Therefore their LHC limits are expected to be stronger than those in MUED. Parameters μ and R^{-1} can be constrained by searches in the dijet [44,45], dilepton [46,47] and W' (lepton + neutrino) [48,49] channels. Previous studies [24,32,33] have explored this aspect in some depth. In particular, the dilepton reach and exclusion are mapped [24] in the (μ, R^{-1}) space for a 10 TeV LHC.

We use CalcHEP [50] and CTEQ 5M PDF to evaluate cross sections. Appropriate cuts and efficiencies have been applied, following experimental studies [44–49]. More accurate calculation depends on detailed mass spectrum of the model, which is currently not known for

³We thank Tom Flacke for pointing out that there are other contributions which arise due to f_2 - f_2 - V_{2n} , f_0 - f_1 - V_{2n+1} , f_0 - f_3 - V_{2n+1} , etc. Individual contributions are expected to be smaller than the leading contribution due to the heaviness of KK fermions. However, summing over all possible KK fermion states, the net contribution may appear divergent. Often the sum is truncated by including KK states up to the corresponding cut off scale times the radius. With this, we think that the total contribution will not change by more than an order of magnitude and will be still below current experimental sensitivity. This issue needs further investigation.

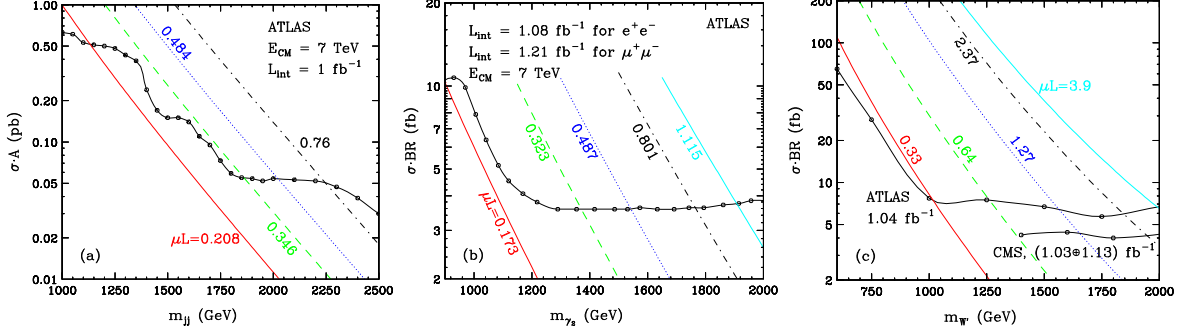


Figure 5: Bounds on masses of KK resonances in dijet (jj in (a)), dilepton ($\ell\ell$ in (b)), and lepton plus missing momentum ($\ell\nu$ in (c)) channels. Curves with circles represent the 95% C.L. upper limit on signal cross sections.

SUED. We here adopt the same mass splittings as in MUED, with $M_{G_2} : M_{W_2} : M_{Z_2} : M_{\gamma_2} \approx 1.3 : 1.07 : 1.07 : 1$, and $M_{\gamma_2} \approx \frac{2}{R}$. Widths of these resonances are computed automatically in CalcHEP. Since all KK fermion final states are prohibited due to their heaviness in most of the parameter space, we only consider SM fermion pairs in the final states. Our results on collider bounds are shown in Fig. 5, with dijet in (a), dilepton in (b), and lepton plus missing momentum in (c). Curves with dots (black-solid) represent the 95% C.L. upper limit on signal cross sections as functions of the relevant resonance mass, while all other curves are signal cross sections in specific channels for various values of bulk mass.

The dijet channel includes resonances through G_2 , γ_2 , Z_2 and W_2 , with a mass spread of $\sim 30\%$ of m_{γ_2} . Production and hadronic decays of different resonances scale the same way with the quark bulk mass μ_Q (but not μ_L). For simplicity, we only consider G_2 , which dominates the others with strong QCD couplings, as well as a larger mass where the background is smaller. We find that in SUED the ATLAS reach is slightly more sensitive to the dijet resonance than the CMS one, therefore we only include the ATLAS analysis below. In Fig. 5(a) we show the 95% C.L. upper limit on cross section times acceptance ($\sigma \times \mathcal{A}$) as a function of the dijet resonance mass. We follow the procedure described in Ref. [44] to set limits on the mass of the dijet resonance. Acceptance is obtained by imposing the suitable kinematic cuts on η , p_T , $|\Delta\eta|$, and invariant mass (m_{jj}) employed in the ATLAS analysis with 1 fb^{-1} . We also include a factor of 0.92 to account for an approximate reduction of acceptance due to the calorimeter readout problem in the region of $\eta \in (-0.1, 1.5)$ and $\phi \in (-0.9, -0.5)$. To compare the 95% C.L. upper limit and our signal cross section, the ratio of the mean mass and the standard deviation of the Gaussian resonance is chosen as 5%, which is the closest value for SUED. Finally the bounds on the dijet invariant mass, $m_{jj} = 1.3 \frac{2}{R}$, can be read off from intersections in Fig. 5(a), and results are translated into the $(\mu R, R^{-1})$ plane, as shown as the magenta-dashed curve in Fig. 3. Note that $\mu L = \mu R \frac{\pi}{2}$.

For the dilepton channel, we include both γ_2 and Z_2 resonances in estimating signal cross sections. μ_Q is important for the production while μ_L is relevant for the decay, although we are considering the universal case in this section. Fig. 5(b) shows the upper limit as a function of dilepton resonance mass ($m_{\ell\ell}$) as well as signal cross sections for various choices of μ .

Note that there are two resonances, γ_2 and Z_2 , with a mass splitting of $m_{Z_2} = 1.07m_{\gamma_2} = 1.07\frac{2}{R}$, and the x -axis represent m_{γ_2} in Fig. 5(b). We use results from ATLAS with an integrated luminosity of 1.08 fb^{-1} in the dielectron channel and 1.21 fb^{-1} in the dimuon channel [46]. Above a resonance mass of 1.2 TeV, their limits stay constant. Translating results to the $(\mu R, R^{-1})$ plane, we find that current LHC bounds in the dilepton channel (red-solid) is similar to that in the dijet channel (magenta-dashed), as shown in Fig. 3. However, as discussed in Ref. [23], the bounds on SUED in the dilepton channel can be improved significantly by including indirect processes, which require a complete knowledge of mass spectrum. The projected bounds assuming 10 times more LHC data are shown as the red-dotted curve.

Finally bounds from the W' search in the lepton plus missing energy channel are shown in Fig. 5 for both ATLAS and CMS, and their corresponding constraints on $(\mu$ and $R^{-1})$ are shown in Fig. 3 (black-dotted). CMS limits are slightly better while ATLAS covers lower mass region. All collider bounds (dijet, dilepton and lepton plus missing energy) constrain regions with large bulk mass and small KK mass scale. Hence the upper-left corner of each curve is ruled out by these searches.

One of our main results is that considering oblique corrections, collider bounds and relic abundance constraints together, SUED parameter space is restricted to a region of $650 \text{ GeV} \lesssim 1/R \lesssim 850 \text{ GeV}$ and $\mu R \lesssim 0.2$ without the resonant annihilation (green band in the left). With the resonance, we are restricted to $750 \lesssim 1/R \lesssim 950 \text{ GeV}$ and $\mu R \lesssim 0.3$ (green band in the right). In general, $\Omega h^2 < 0.1123$ is still acceptable, in which case the yellow-shaded region is allowed. Considering current performance of the LHC, the remaining parameter space of the universal bulk-mass will be highly constrained. For example, the dilepton resonance search with 10 fb^{-1} will be sensitive down to $\mu R \lesssim 0.1-0.2$.

4. A Non-Universal Case: $\mu_L \neq \mu_Q$

Once we remove the universal bulk mass requirement, fermions can take on more generic flavor and chiral structures. To avoid stringent bounds from the flavor changing neutral current (FCNC) effects, and for simplicity, we consider the case where all leptons have the same bulk mass μ_L and all quarks μ_Q . The constraints on the full parameter space of such model, (μ_L, μ_Q, R^{-1}) , are considered in this section.

With different mass parameters μ_L for leptons and μ_Q for quarks, the bound on μ_Q can be substantially weakened, because for $\mu_L = 0$, the couplings of the muon to non-zero KK W modes vanish, and muon decay only proceeds via the W zero-mode. In fact, for non-universal masses $\mu_L \neq \mu_Q$, leptonic and hadronic channels at LEP are not affected universally any more, so that a treatment in terms of the oblique (S, T, U) parameters is insufficient, and a global fit to the LEP data is required for a reliable electroweak analysis, which we reserve for future study. However we still can find quite tight bounds on the parameter space by considering the potentially relevant constraints coming from corrections to the decay rate of muon in terms of Fermi constant (δG_F), and from the four Fermi contact interactions of

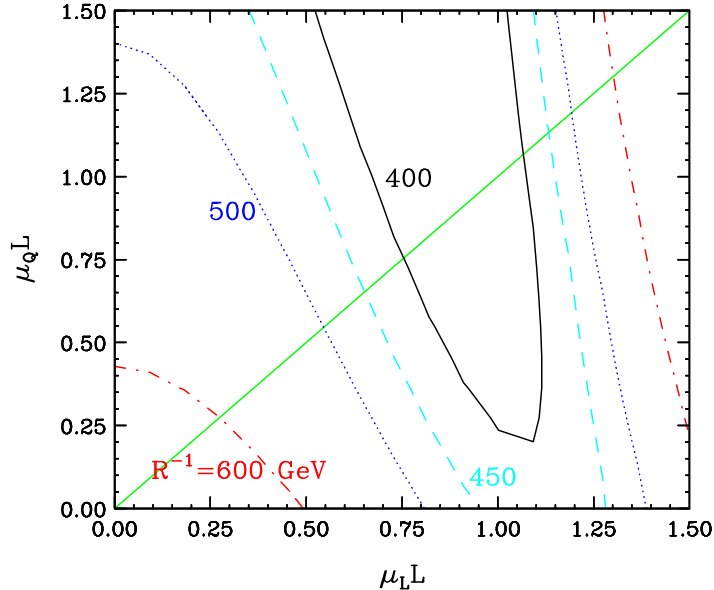


Figure 6: Oblique corrections in the case of two fermion-bulk masses. Each contour disfavors its outside region for a given R^{-1} (99% C.L.). The universal case is along the green line ($\mu_L = \mu_Q$).

various types. We also consider the anomalous magnetic moment of muon, which currently is known to have a slight disagreement between the theoretical and experimental values.

4.1 Electroweak Precision Measurements: Oblique Corrections, Four Fermi Operators and Anomalous Magnetic Moment

Unlike the universal case ($\mu_L = \mu_Q$) in section 3.1, the analysis with oblique parameters (S, T, U) may not provide enough information on the new physics effects as non-universal corrections to couplings are involved. However, we still find a stringent bound in the non-universal case using an effective parametrization of oblique corrections as follows: For $(S, T, U)_{\text{UED}}$, the loop contributions from KK tops are again the most relevant among all fermion contributions due to the fermion mass suppression in Eq. (3.8). The most important constraint for δG_F is from the precise measurement of the muon decay process, for which the leading order correction vanishes when $\mu_L = 0$ regardless the value of μ_Q . Capturing these facts we conveniently replace $\mu \rightarrow \mu_Q$ for $(S, T, U)_{\text{UED}}$ and $\mu \rightarrow \mu_L$ for δG_F as leading order contributions. Then we use the oblique parameter fits and correlation matrix from the *Gfitter* collaboration [13].

Fig. 6 shows contours of R^{-1} that are consistent with EW observables in the (μ_L, μ_Q) plane at 99% C.L. Each contour disfavors its region outside. The universal bulk-mass case can be obtained by taking limits along the diagonal line (in green). For instance, taking the contour of $R^{-1} = 500$ GeV, one can read off the allowed ranges of $\mu_Q L = \mu_L L \in [0.545, 1.192]$ ($\mu_Q R = \mu_L R \in [0.347, 0.759]$), which is consistent with the universal case as shown in Fig. 3.

As oblique corrections may not capture the full features of corrections, we also wish to

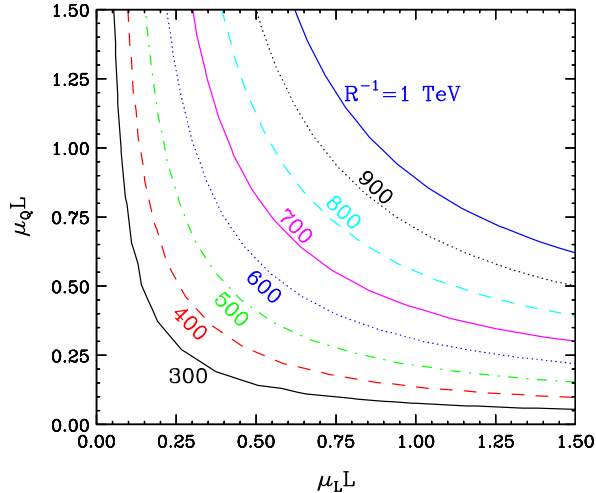


Figure 7: Four Fermi Interaction (from *eedd*) constrains the upper-right corner for a given R^{-1} .

include four Fermi contact operators. Actually the tree level 0-0-(2n) interactions could be large enough in the presence of bulk masses to greatly enhance the contact interactions. To analyze four Fermi operators, we can generalize Eq. (3.14) for $\mu_L \neq \mu_Q$ case, simply by replacing $(\mathcal{F}_{00}^{2n}(\mu R))^2$ with $\mathcal{F}_{00}^{2n}(\mu_Q R)\mathcal{F}_{00}^{2n}(\mu_L R)$. \mathcal{F}_{00}^{2n} increases as μ increases so that the upper-right corner of (μ_L, μ_Q) plane is constrained by the four Fermi interactions. In Fig. 7 we show bounds from *eedd* operator, which is the most stringent among all operators we consider (see Table 1). For a given point (μ_L, μ_Q) , one can read off lower bound on R^{-1} . For example, for $\mu_L L \approx 1 \approx \mu_Q L$, $R^{-1} \lesssim 1$ TeV is ruled out but if one of the bulk mass parameter becomes small a quite large portion of the parameter space is still available.

In the leading order approximation, the anomalous muon magnetic moment is only sensitive to μ_L so that the non-universal case with $\mu_L \neq \mu_Q$ does not add more information other than that in section 3.4.

4.2 Relic Abundance of KK Photon

We show our results on relic density in Fig. 8, where contours represent values of R^{-1} that lead to $\Omega h^2 = 0.1123$ without (with) h_2 resonance in (a) (in (b)). In the calculation of relic abundance, two bulk masses factor in differently in each fermion sector. Requiring that KK photon accounts for all of the dark matter in our universe ($\Omega h^2 = 0.1123$) leads to indirect exclusion. KK photon is mostly the KK partner of the hypercharge gauge boson and couples to leptons stronger than to quarks due to larger hypercharges of leptons. We therefore notice that μ_L is more constrained than μ_Q .

For a given set of (μ_L, μ_Q) , the contours serve as an upper bound on allowed R^{-1} . Any value larger than R^{-1} would have a problem with overclosure. For instance, $(\mu_L L, \mu_Q L) = (1, 1)$ denoted by a circle (in red) in Fig. 8(b) is allowed and the corresponding value of contour is about 600 GeV for $\Omega h^2 = 0.1123$. Therefore we learn that the model point, $(\mu_L L, \mu_Q L) = (1, 1)$, is not allowed for $R^{-1} > 600$ GeV. In principle, $R^{-1} < 600$ GeV

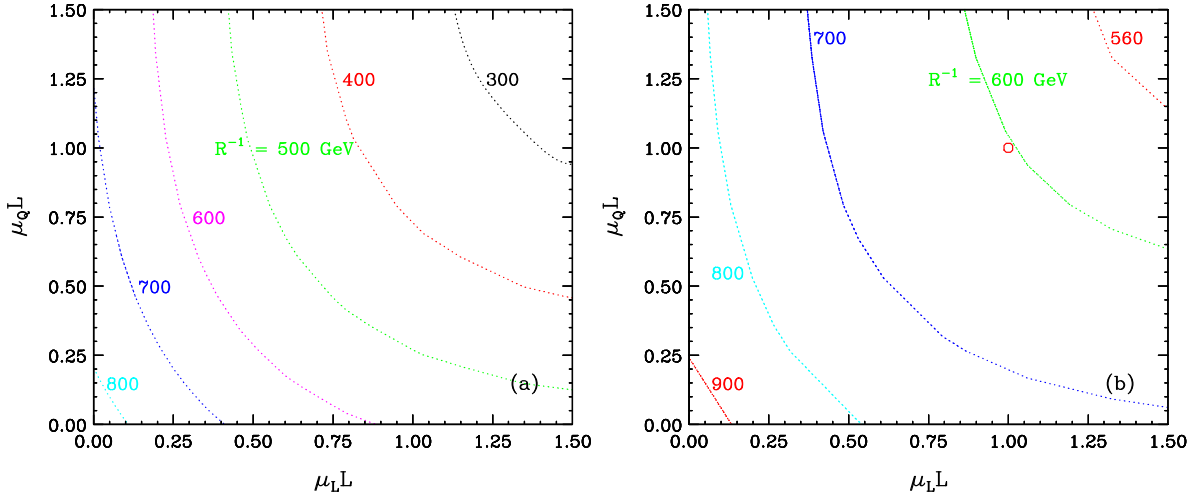


Figure 8: Relic abundance for two bulk masses, μ_Q and μ_L for quark and lepton sector, respectively. Contours represent values of R^{-1} that lead to $\Omega h^2 = 0.1123$ without (with) h_2 resonance in (a) (in (b)). For a given set of (μ_L, μ_Q) , the contours serve as an upper bound on allowed R^{-1} .

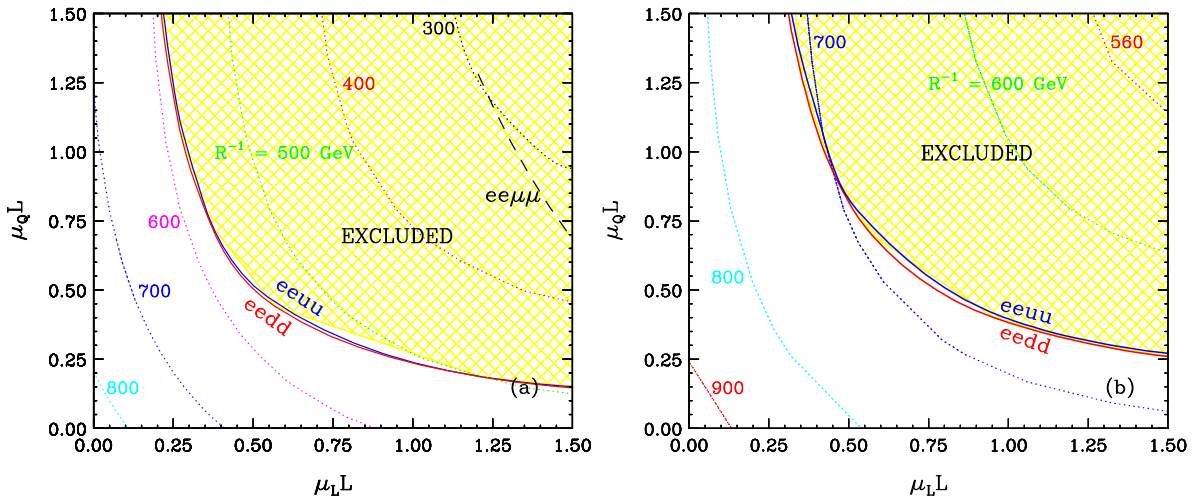


Figure 9: Four Fermi Interaction combined with relic density without (with) h_2 resonance in (a) (in (b)).

for $(\mu_L L, \mu_Q L) = (1, 1)$ can still be consistent with cosmological observation but one needs multiple dark matter candidates to make up the difference.

In Fig. 9 we depict the bounds from the four Fermi contact interactions (especially the operators $eedd, eeuu, ee\mu\mu$) combined with relic density without (with) h_2 resonance. A slightly larger parameter space survives when the h_2 resonance is effective.

4.3 Collider Bounds

In the non-universal bulk mass case, both dilepton and W' channels constrain the model in the full (μ_Q, μ_L, R^{-1}) parameter space, while the dijet channel only constrain (μ_Q, R^{-1}) .

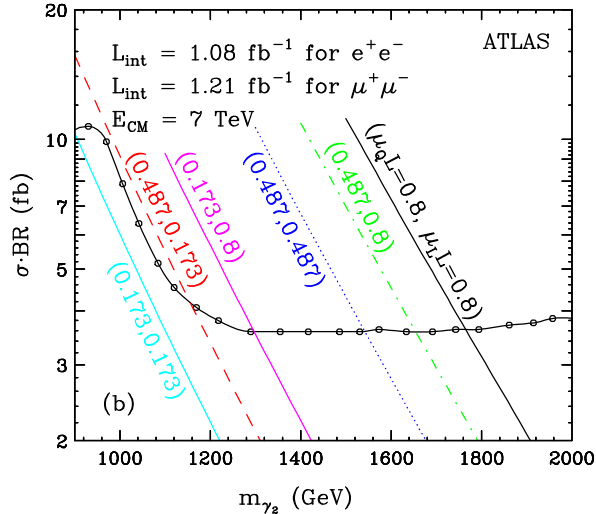


Figure 10: Bounds on the masses of KK resonances in the dilepton ($\ell\ell$) channel. The curve with dots represents the 95% C.L. upper limit on signal cross sections.

Since the W' bound is weaker than the dilepton one as demonstrated in the universal bulk mass case in section 3.5, we here consider the dijet and dilepton channels only.

We would like to emphasize that when the bulk lepton masses are vanishingly small $\mu_L R \ll 1$, the second KK modes of the electroweak gauge bosons cannot contribute to s -channel exchange at tree-level in the dilepton channel, which serves as one of the main search channels for UED and its extensions at the LHC.

In Fig. 10, we show the 95% C.L. upper limit on signal cross sections (black, solid with dots), as well as signal cross sections for various choices of (μ_Q, μ_L) . As expected, dilepton bounds in this case can be stronger or weaker depending on the magnitude of μ_Q and μ_L . For instance, for a fixed value of $\mu_Q L = 0.487$, the corresponding mass bound for increasing $\mu_L L$ (from 0.173 to 0.487, 0.8) also grows stronger (from 1150 to 1550, 1650 GeV) (see three curves in red-dashed, blue-dotted, and green-dot-dashed for comparison). The dilepton limit, on the other hand, is in fact a 2-dimensional ‘exclusion surface’ in the (μ_Q, μ_L, R^{-1}) space. We recall that the relic abundance requirement $\Omega h^2 = 0.1123$ also corresponds to a 2-dimensional ‘constraint surface’. By intersecting these two surfaces and projecting down to the (μ_Q, μ_L) plane, we obtain the dilepton exclusion curves in Fig. 11. We also include the projected dilepton limit with 10 fb^{-1} at ATLAS.

The dijet exclusion limits are identical to those in the universal bulk mass case if we replace μ with μ_Q , as shown in Fig. 3 but in the (μ_Q, R^{-1}) plane, instead. We can promote the exclusion curve to 2 dimensional ‘exclusion surface’ as well, by sweeping it through the μ_L direction. Intersecting the resultant surface with the relic abundance surface yields the dijet exclusion curves in Fig. 11. The dilepton limit is more stringent than the dijet limit with relatively large μ_L . At small μ_L , the dijet limit dominates, excluding μ_Q above 0.7 (0.4) for vanishing $\mu_L L$ in the case with (without) resonance annihilation. In the case of resonant annihilation, we do not show the CDF dijet limit in Fig. 11(b), since it is completely inside

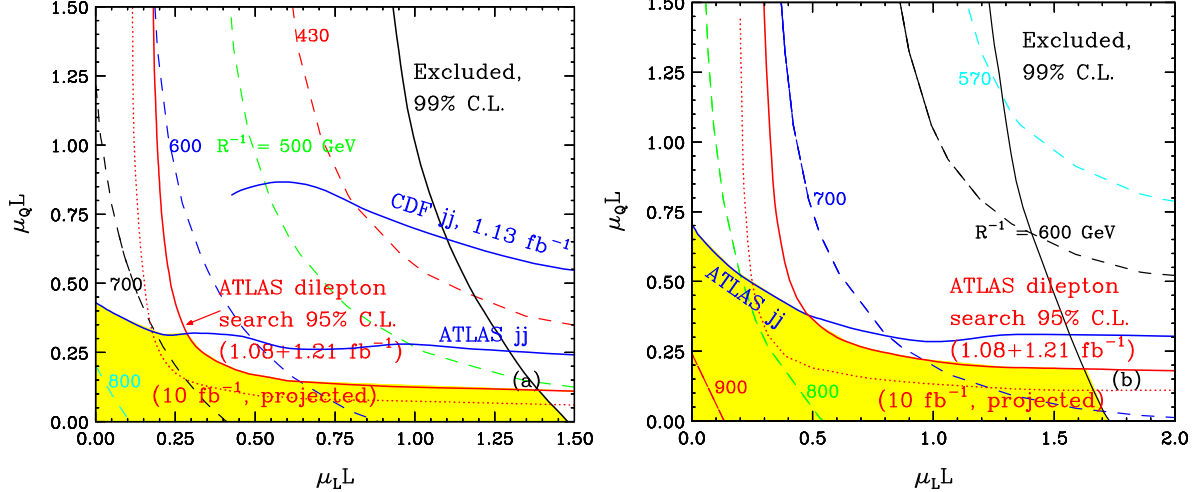


Figure 11: Relic abundance, electroweak and collider constraints for two bulk masses. Contours represent values of R^{-1} that lead to $\Omega h^2 = 0.1123$ without (with) h_2 resonance in (a) (in (b)). Region in the right side of black curve (labeled as “Excluded”) is disfavored by oblique corrections (99% C.L.) for $\Omega h^2 = 0.1123$. The red curves represent exclusion limit from current (solid) and projected 10 fb^{-1} (dotted) ATLAS dilepton search. The dijet constraints are shown in blue-solid curves. Dashed curves represent contours of R^{-1} that is consistent with $\Omega h^2 = 0.1123$. Note that $L = \pi R/2$.

the region excluded by oblique corrections plus relic density.

If the oblique correction fit C.L. is lowered from 99%, the excluded regions in Fig. 11 expand. In the no-resonance case at 95% C.L., an additional excluded ‘island’ region (not shown) appears near $\mu_Q L \sim \mu_L L \sim 0.5$ with $R^{-1} \sim 600 \text{ GeV}$, corresponding to the portion of the ‘a’ relic density curve near $\mu_R \sim 0.3$ and $R^{-1} \sim 600 \text{ GeV}$ in Fig. 3 that is excluded by the 95% C.L. oblique fit contour. As we lower the fit C.L., this island region grows along the diagonal line and eventually merges with the ‘mainland’ exclusion. In the resonance case, there is no such ‘island’ feature for any C.L. fit we consider.

Overall, the SUED model with 2 bulk masses is also strongly constrained. The yellow-shaded region in Fig. 11 shows the allowed space, which is bounded by electroweak precision constraints and relic abundance at relatively large μ_L , and by collider dijet limit at small μ_L . In between they are bridged by limits from the dilepton search. The UED scale R^{-1} is constrained to be between 500-850 GeV without h_2 resonance annihilation. With resonance, the range is raised to between 650-950 GeV.

5. Summary and Outlook

In general vectorlike fermion-bulk masses could be introduced in models with universal extra dimensions, and lead to significant changes in dark matter and collider phenomenology. They could shift all KK fermion masses and induce tree-level couplings between even numbered KK gauge bosons and SM fermions. They still preserve KK parity, providing a viable dark

matter candidate. Models with fermion-bulk masses resemble Split SUSY in the sense that partners of SM fermions are heavy.

We restricted ourselves to the case of positive bulk mass, to keep KK photon as a dark matter. In principle, negative bulk mass is also allowed, in which case KK fermions get negative corrections in masses and KK neutrinos will likely be a dark matter candidate. However, direct detection experiments disfavor KK neutrino dark matter due to large elastic scattering cross sections.

In this paper, we have investigated various constraints including oblique corrections, four Fermi interactions, relic abundance and collider bounds. As in the case of MUED, we find a tension between electroweak precision constraints and relic abundance of KK photon for the universal fermion-bulk mass term. The remaining parameter space is highly constrained by searches at colliders. As a result, we find the allowed region within $\mu R \lesssim 0.2-0.3$ and $650 \text{ GeV} \lesssim R^{-1} \lesssim 950 \text{ GeV}$. Precise calculation of the relic abundance with 1-loop corrected mass spectrum including all coannihilations and relevant resonances may slightly broaden the allowed range for the universal bulk mass term. However, considering performance of the LHC, the tension still exists and the universal bulk mass is disfavored.

This tension may be relieved by introducing separate bulk masses for the quark and lepton sectors. In this scenario, dijet searches at the LHC together with relic abundance set strong bounds on the bulk parameter in the quark sector, $\mu_Q L \lesssim 0.7$ ($\mu_Q R \lesssim 0.45$), while upper limit on the bulk mass in the lepton sector is given by a combination of relic abundance and oblique corrections, $\mu_L L \lesssim 1.7$ ($\mu_L R \lesssim 1.1$). The LHC is expected to play an important role in constraining the remaining parameter space.

Finally we note that a treatment in terms of the oblique (S, T, U) parameters may be insufficient, and a global fit to the experimental data is required for a reliable electroweak analysis, although our results on oblique corrections contain main features of electroweak constraints.

Acknowledgments

We thank Thomas Flacke for valuable discussion and comments on manuscript. GH is supported by the US DOE Grant Number DE-FG02-04ER14308. KK is supported in part by the University of Kansas General Research Fund allocation 2301566, by the National Science Foundation under Award No. EPS-0903806 and matching funds from the State of Kansas through the Kansas Technology Enterprise Corporation. SC is supported by Basic Science Research Program through the National Research Foundation of Korea funded by the Ministry of Education, Science and Technology (2011-0010294) and (2011-0029758).

References

- [1] T. Appelquist, H. C. Cheng and B. A. Dobrescu, “Bounds on universal extra dimensions,” *Phys. Rev. D* **64** (2001) 035002 [arXiv:hep-ph/0012100].
- [2] H. -C. Cheng, K. T. Matchev and M. Schmaltz, “Radiative corrections to Kaluza-Klein masses,” *Phys. Rev. D* **66**, 036005 (2002) [hep-ph/0204342].

- [3] H. -C. Cheng, K. T. Matchev and M. Schmaltz, “Bosonic supersymmetry? Getting fooled at the CERN LHC,” *Phys. Rev. D* **66**, 056006 (2002) [hep-ph/0205314].
- [4] D. Hooper and S. Profumo, “Dark matter and collider phenomenology of universal extra dimensions,” *Phys. Rept.* **453**, 29 (2007) [arXiv:hep-ph/0701197].
- [5] A. Datta, K. Kong and K. T. Matchev, “Minimal Universal Extra Dimensions in CalcHEP/CompHEP,” *New J. Phys.* **12**, 075017 (2010) [arXiv:1002.4624 [hep-ph]].
- [6] K. Kong, K. Matchev and G. Servant, “Extra Dimensions at the LHC,” In *Bertone, G. (ed.): Particle dark matter* 306-324 [arXiv:1001.4801 [hep-ph]].
- [7] B. Bhattacharjee and K. Ghosh, “Search for the minimal universal extra dimension model at the LHC with $\sqrt{s}=7$ TeV,” *Phys. Rev. D* **83**, 034003 (2011) [arXiv:1006.3043 [hep-ph]];
H. Murayama, M. M. Nojiri and K. Tobioka, “Improved discovery of a nearly degenerate model: MUED using MT2 at the LHC,” *Phys. Rev. D* **84**, 094015 (2011) [arXiv:1107.3369 [hep-ph]];
A. Datta, A. Datta and S. Poddar, “Enriching the exploration of the MUED model with event shape variables at the CERN LHC,” arXiv:1111.2912 [hep-ph].
- [8] S. Arrenberg, L. Baudis, K. Kong, K. T. Matchev and J. Yoo, “Kaluza-Klein Dark Matter: Direct Detection vis-a-vis LHC,” *Phys. Rev. D* **78**, 056002 (2008) [arXiv:0805.4210 [hep-ph]].
- [9] G. Bertone, K. Kong, R. R. de Austri and R. Trotta, “Global fits of the Minimal Universal Extra Dimensions scenario,” *Phys. Rev. D* **83**, 036008 (2011) [arXiv:1010.2023 [hep-ph]].
- [10] A. J. Buras, M. Spranger and A. Weiler, “The impact of universal extra dimensions on the unitarity triangle and rare K and B decays.,” *Nucl. Phys. B* **660** (2003) 225 [arXiv:hep-ph/0212143];
A. J. Buras, A. Poschenrieder, M. Spranger and A. Weiler, “The impact of universal extra dimensions on $B \rightarrow X/s$ gamma, $B \rightarrow X/s$ gluon, $B \rightarrow X/s$ $\mu^+ \mu^-$, $K(L) \rightarrow \pi^0 e^+ e^-$, and ϵ'/ϵ ,” *Nucl. Phys. B* **678** (2004) 455 [arXiv:hep-ph/0306158];
U. Haisch and A. Weiler, “Bound on minimal universal extra dimensions from anti- $B \rightarrow X/s$ gamma,” *Phys. Rev. D* **76**, 034014 (2007) [arXiv:hep-ph/0703064];
P. Colangelo, F. De Fazio, R. Ferrandes and T. N. Pham, “Exclusive $B \rightarrow K^{(*)} l^+ l^-$, $B \rightarrow K^{(*)} \nu \text{ anti-}\nu$ and $B \rightarrow K^* \text{ gamma}$ transitions in a scenario with a single universal extra dimension,” *Phys. Rev. D* **73**, 115006 (2006) [arXiv:hep-ph/0604029];
P. Colangelo, F. De Fazio, R. Ferrandes and T. N. Pham, “Spin effects in rare $B \rightarrow X/s$ $\tau^+ \tau^-$ and $B \rightarrow K^* \tau^+ \tau^-$ decays in a single universal extra dimension scenario,” *Phys. Rev. D* **74**, 115006 (2006) [arXiv:hep-ph/0610044];
T. M. Aliev and M. Savci, “ $\Lambda/b \rightarrow \Lambda l^+ l^-$ decay in universal extra dimensions,” *Eur. Phys. J. C* **50**, 91 (2007) [arXiv:hep-ph/0606225].
- [11] T. Appelquist and H. U. Yee, “Universal extra dimensions and the Higgs boson mass,” *Phys. Rev. D* **67** (2003) 055002 [arXiv:hep-ph/0211023].
- [12] I. Gogoladze and C. Macesanu, “Precision electroweak constraints on universal extra dimensions revisited,” *Phys. Rev. D* **74**, 093012 (2006) [arXiv:hep-ph/0605207].
- [13] M. Baak *et al.* [The G-fitter Group], “Updated Status of the Global Electroweak Fit and Constraints on New Physics,” arXiv:1107.0975 [hep-ph].

- [14] G. Servant and T. M. P. Tait, “Is the lightest Kaluza-Klein particle a viable dark matter candidate?,” Nucl. Phys. B **650** (2003) 391 [arXiv:hep-ph/0206071].
- [15] H. -C. Cheng, J. L. Feng and K. T. Matchev, “Kaluza-Klein dark matter,” Phys. Rev. Lett. **89**, 211301 (2002) [hep-ph/0207125].
- [16] K. Kong and K. T. Matchev, “Precise calculation of the relic density of Kaluza-Klein dark matter in universal extra dimensions,” JHEP **0601**, 038 (2006) [hep-ph/0509119].
- [17] G. Belanger, M. Kakizaki and A. Pukhov, “Dark matter in UED: The Role of the second KK level,” JCAP **1102**, 009 (2011) [arXiv:1012.2577 [hep-ph]].
- [18] M. Kakizaki, S. Matsumoto and M. Senami, “Relic abundance of dark matter in the minimal universal extra dimension model,” Phys. Rev. D **74**, 023504 (2006) [hep-ph/0605280].
- [19] M. Kakizaki, S. Matsumoto, Y. Sato and M. Senami, “Relic abundance of LKP dark matter in UED model including effects of second KK resonances,” Nucl. Phys. B **735**, 84 (2006) [hep-ph/0508283].
- [20] M. Kakizaki, S. Matsumoto, Y. Sato and M. Senami, “Significant effects of second KK particles on LKP dark matter physics,” Phys. Rev. D **71**, 123522 (2005) [hep-ph/0502059].
- [21] G. R. Dvali, G. Gabadadze, M. Kolanovic and F. Nitti, “The power of brane-induced gravity,” Phys. Rev. D **64**, 084004 (2001) [arXiv:hep-ph/0102216];
M. S. Carena, T. M. P. Tait and C. E. M. Wagner, “Branes and orbifolds are opaque,” Acta Phys. Polon. B **33** (2002) 2355 [arXiv:hep-ph/0207056];
F. del Aguila, M. Perez-Victoria and J. Santiago, “Bulk fields with general brane kinetic terms,” JHEP **0302**, 051 (2003) [arXiv:hep-th/0302023];
F. del Aguila, M. Perez-Victoria and J. Santiago, “Effective description of brane terms in extra dimensions,” JHEP **0610**, 056 (2006) [arXiv:hep-ph/0601222];
T. Flacke, A. Menon and D. J. Phalen, “Non-minimal universal extra dimensions,” Phys. Rev. D **79**, 056009 (2009) [arXiv:0811.1598 [hep-ph]].
- [22] S. C. Park and J. Shu, “Split Universal Extra Dimensions and Dark Matter,” Phys. Rev. D **79**, 091702 (2009) [arXiv:0901.0720 [hep-ph]].
- [23] A. Datta, K. Kong and K. T. Matchev, “Discrimination of supersymmetry and universal extra dimensions at hadron colliders,” Phys. Rev. D **72**, 096006 (2005) [Erratum-ibid. D **72**, 119901 (2005)] [hep-ph/0509246].
- [24] K. Kong, S. C. Park and T. G. Rizzo, “Collider Phenomenology with Split-UED,” JHEP **1004**, 081 (2010) [arXiv:1002.0602 [hep-ph]].
- [25] D. Kim, Y. Oh and S. C. Park, “W’ in new physics models at the LHC,” arXiv:1109.1870 [hep-ph].
- [26] L. Edelhauser, W. Porod and R. K. Singh, “Spin Discrimination in Three-Body Decays,” JHEP **1008**, 053 (2010) [arXiv:1005.3720 [hep-ph]].
- [27] T. Flacke and C. Pasold, “Constraints on split-UED from Electroweak Precision Tests,” arXiv:1111.7250 [hep-ph].
- [28] C. Csaki, J. Heinonen, J. Hubisz, S. C. Park and J. Shu, “5D UED: Flat and Flavorless,” JHEP **1101**, 089 (2011) [arXiv:1007.0025 [hep-ph]].

- [29] G. Cacciapaglia, C. Csaki, C. Grojean, M. Reece and J. Terning, “Top and bottom: A Brane of their own,” *Phys. Rev. D* **72**, 095018 (2005) [hep-ph/0505001].
- [30] K. Agashe, A. Falkowski, I. Low and G. Servant, “KK Parity in Warped Extra Dimension,” *JHEP* **0804**, 027 (2008) [arXiv:0712.2455 [hep-ph]].
- [31] H. Georgi, A. K. Grant and G. Hailu, “Chiral fermions, orbifolds, scalars and fat branes,” *Phys. Rev. D* **63**, 064027 (2001) [hep-ph/0007350].
- [32] C. -R. Chen, M. M. Nojiri, S. C. Park, J. Shu and M. Takeuchi, “Dark matter and collider phenomenology of split-UED,” *JHEP* **0909**, 078 (2009) [arXiv:0903.1971 [hep-ph]].
- [33] K. Kong, S. C. Park and T. G. Rizzo, “A vector-like fourth generation with a discrete symmetry from Split-UED,” *JHEP* **1007**, 059 (2010) [arXiv:1004.4635 [hep-ph]].
- [34] H. Dohi and K. -y. Oda, “Universal Extra Dimensions on Real Projective Plane,” *Phys. Lett. B* **692**, 114 (2010) [arXiv:1004.3722 [hep-ph]];
G. Cacciapaglia, A. Deandrea and J. Llodra-Perez, “The Universal Real Projective Plane: LHC phenomenology at one Loop,” *JHEP* **1110**, 146 (2011) [arXiv:1104.3800 [hep-ph]].
- [35] T. Appelquist, B. A. Dobrescu, E. Ponton and H. -U. Yee, “Proton stability in six-dimensions,” *Phys. Rev. Lett.* **87**, 181802 (2001) [hep-ph/0107056];
G. Burdman, B. A. Dobrescu and E. Ponton, “Six-dimensional gauge theory on the chiral square,” *JHEP* **0602**, 033 (2006) [hep-ph/0506334];
G. Burdman, B. A. Dobrescu and E. Ponton, “Resonances from two universal extra dimensions,” *Phys. Rev. D* **74**, 075008 (2006) [hep-ph/0601186].
- [36] M. E. Peskin and T. Takeuchi, “A New constraint on a strongly interacting Higgs sector,” *Phys. Rev. Lett.* **65**, 964 (1990).
- [37] M. S. Carena, E. Ponton, T. M. P. Tait and C. E. MWagner, “Opaque branes in warped backgrounds,” *Phys. Rev. D* **67**, 096006 (2003) [hep-ph/0212307];
T. G. Rizzo and J. D. Wells, “Electroweak precision measurements and collider probes of the standard model with large extra dimensions,” *Phys. Rev. D* **61**, 016007 (2000) [hep-ph/9906234];
H. Davoudiasl, J. L. Hewett and T. G. Rizzo, “Bulk gauge fields in the Randall-Sundrum model,” *Phys. Lett. B* **473**, 43 (2000) [hep-ph/9911262];
C. Csaki, J. Erlich and J. Terning, “The Effective Lagrangian in the Randall-Sundrum model and electroweak physics,” *Phys. Rev. D* **66**, 064021 (2002) [hep-ph/0203034].
- [38] G. Servant and T. M. P. Tait, “Elastic scattering and direct detection of Kaluza-Klein dark matter,” *New J. Phys.* **4**, 99 (2002) [hep-ph/0209262].
- [39] E. Aprile *et al.* [XENON100 Collaboration], “Dark Matter Results from 100 Live Days of XENON100 Data,” *Phys. Rev. Lett.* **107**, 131302 (2011) [arXiv:1104.2549 [astro-ph.CO]].
- [40] G. -C. Cho, K. Hagiwara and S. Matsumoto, *Eur. Phys. J. C* **5**, 155 (1998) [hep-ph/9707334].
- [41] K. Nakamura *et al.* (Particle Data Group), *J. Phys. G* **37**, 075021 (2010) and 2011 partial update for the 2012 edition.
- [42] T. Appelquist and B. A. Dobrescu, “Universal extra dimensions and the muon magnetic moment,” *Phys. Lett. B* **516**, 85 (2001) [hep-ph/0106140].

- [43] F. Jegerlehner and A. Nyffeler, “The Muon $g-2$,” Phys. Rept. **477**, 1 (2009) [arXiv:0902.3360 [hep-ph]].
- [44] G. Aad *et al.* [ATLAS Collaboration], “Search for New Physics in the Dijet Mass Distribution using 1 fb^{-1} of pp Collision Data at $\sqrt{s} = 7 \text{ TeV}$ collected by the ATLAS Detector,” Phys. Lett. B **708**, 37 (2012) [arXiv:1108.6311 [hep-ex]].
- [45] S. Chatrchyan *et al.* [CMS Collaboration], “Search for Resonances in the Dijet Mass Spectrum from 7 TeV pp Collisions at CMS,” Phys. Lett. B **704**, 123 (2011) [arXiv:1107.4771 [hep-ex]].
- [46] G. Aad *et al.* [ATLAS Collaboration], “Search for dilepton resonances in pp collisions at $\sqrt{s} = 7 \text{ TeV}$ with the ATLAS detector,” Phys. Rev. Lett. **107**, 272002 (2011) [arXiv:1108.1582 [hep-ex]].
- [47] S. Chatrchyan *et al.* [CMS Collaboration], “Search for Resonances in the Dilepton Mass Distribution in pp Collisions at $\sqrt{s} = 7 \text{ TeV}$,” JHEP **1105**, 093 (2011) [arXiv:1103.0981 [hep-ex]].
- [48] G. Aad *et al.* [ATLAS Collaboration], “Search for a heavy gauge boson decaying to a charged lepton and a neutrino in 1 fb^{-1} of pp collisions at $\sqrt{s} = 7 \text{ TeV}$ using the ATLAS detector,” Phys. Lett. B **705**, 28 (2011) [arXiv:1108.1316 [hep-ex]].
- [49] CMS Collaboration, “Search for W' in the leptonic channels in pp collisions at $\sqrt{s} = 7 \text{ TeV}$,” CMS PAS EXO-11-024
- [50] A. Pukhov, “CalcHEP 2.3: MSSM, structure functions, event generation, batchs, and generation of matrix elements for other packages,” hep-ph/0412191.